Supporting Material for:

The Lipooligosaccharide of the Gut Symbiont *Akkermansia muciniphila* Exhibits A Remarkable Structure and TLR Signaling Capacity

Supplementary Figures

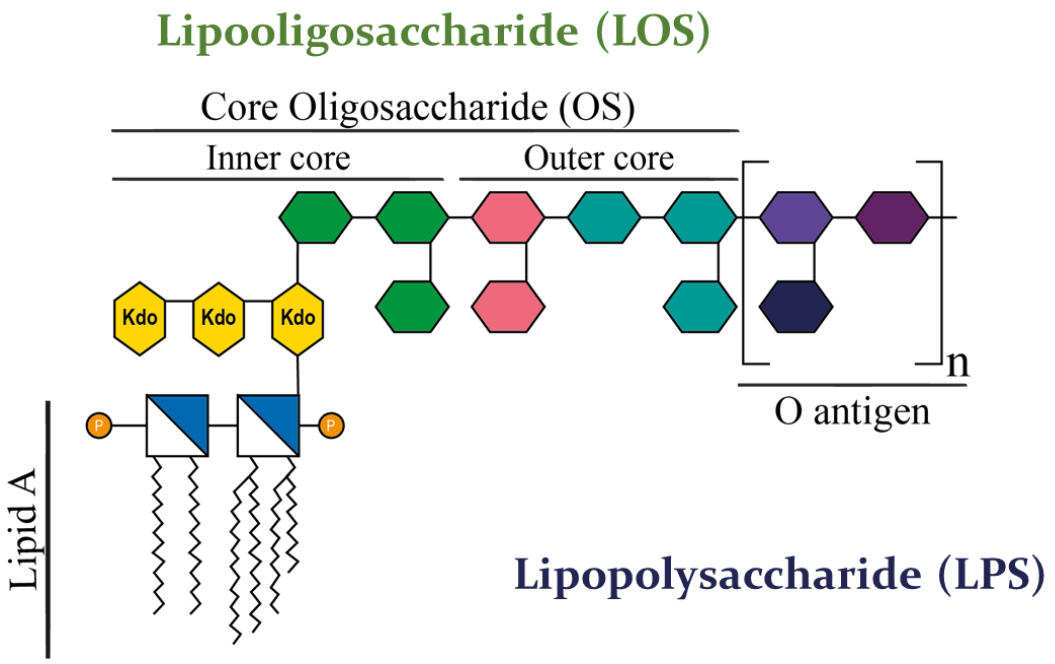

Fig. S1. General structure of a bacterial lipopolysaccharide: consisting out of a Lipid A, a core Oligosaccharide (inner and outer core) and a repeated O-Antigen unit. LOS, or Lipooligosaccharide units typically consist out of the same structural parts, except for the repetitive O-antigen structure.

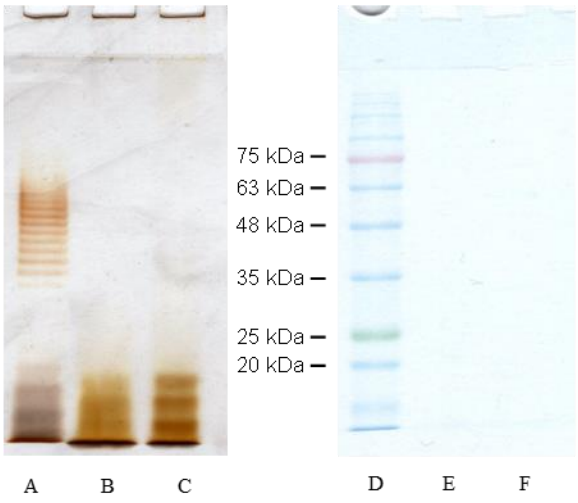

Fig. S2. SDS-PAGE with silver staining of the purified LOS. **SDS-PAGE of the purified LOS**. *A. muciniphila* Muc^T dried cells (8 g) were treated by a combination of the phenol/chloroform/light petroleum (PCP) and the hot phenol/water extractions to isolate the LOS. The silver-stained gel showed the presence of LOS in both phases resulting from the PCP extraction and the water phase of the hot phenol/water extraction. Subsequently, the samples underwent an enzymatic digestion followed by centrifugation and ultracentrifugation. Then, they underwent the Hirschfeld *et al.* protocol to ensure the removal of lipoproteins possibly present followed by inspection via SDS-PAGE and Coomassie Brilliant Blue staining. **A**. *E. coli* O127:B8 LPS (Merck); **B.** *A. muciniphila* LOS obtained from water phase of the hot phenol/water extraction; **C**. *A. muciniphila* LOS obtained from PCP extraction. **D.** BLUeye Prestained Protein Ladder (2 µL) (Merck); **E.** *A. muciniphila* LOS from water phase after Hirschfeld *et al.* protocol; **F.** *A. muciniphila* LOS from PCP extraction after Hirschfeld *et al.* protocol. For **A**, **B**, and **C**, 8 µL of a 1 mg/mL solution of each LOS was loaded onto the gel. For **E** and **F**, 40 µL of a 1 mg/mL solution of each purified LOS was loaded onto the gel. (Abbreviations used: LPS = lipopolysaccharide, LOS = lipooligosaccharide)

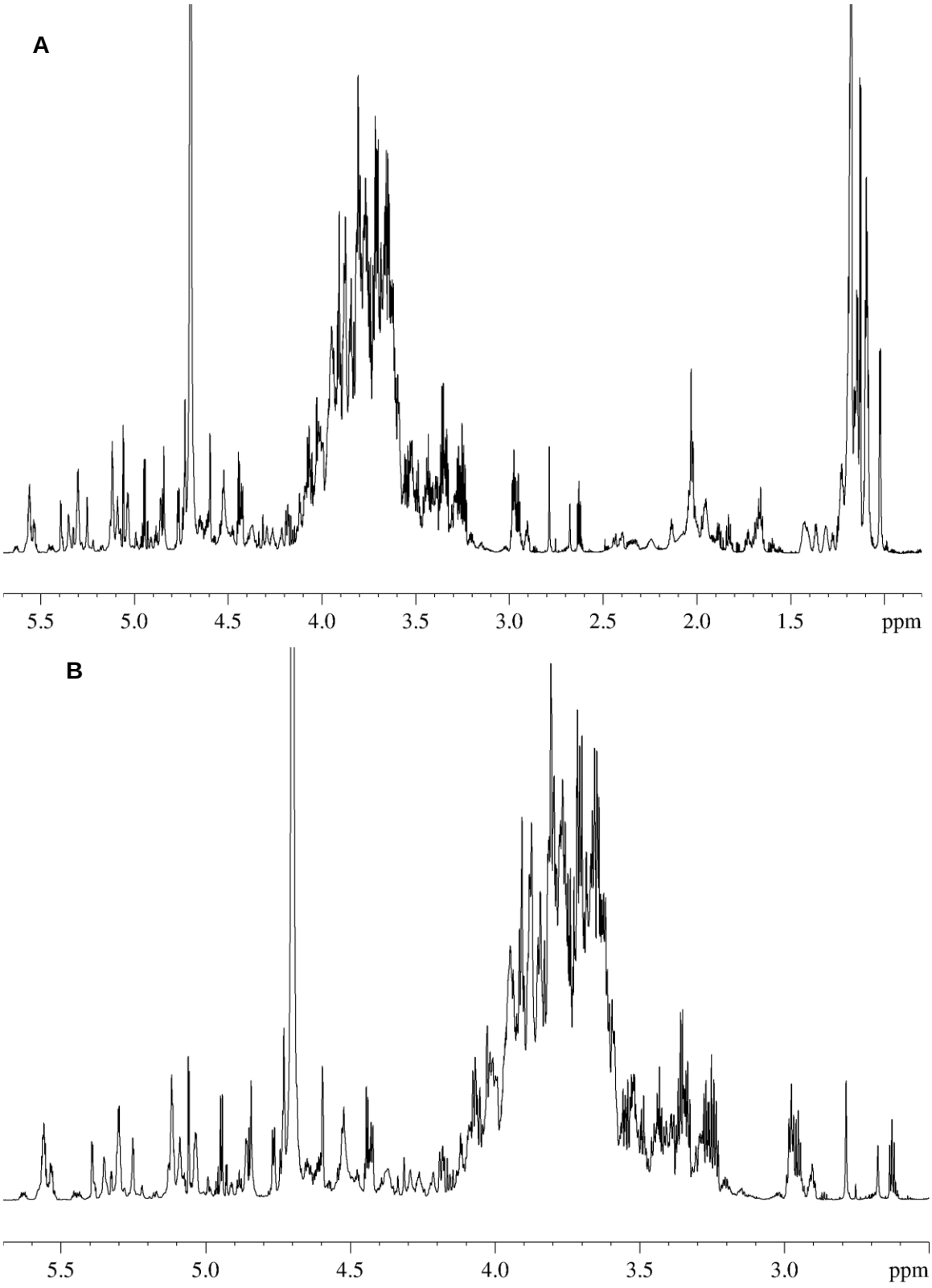
A
5.5
5.0
4.5
4.0
3.5
3.0
2.5
2.0
1.5
ppm
B
5.5
5.0
4.5
4.0
3.5
3.0
ppm

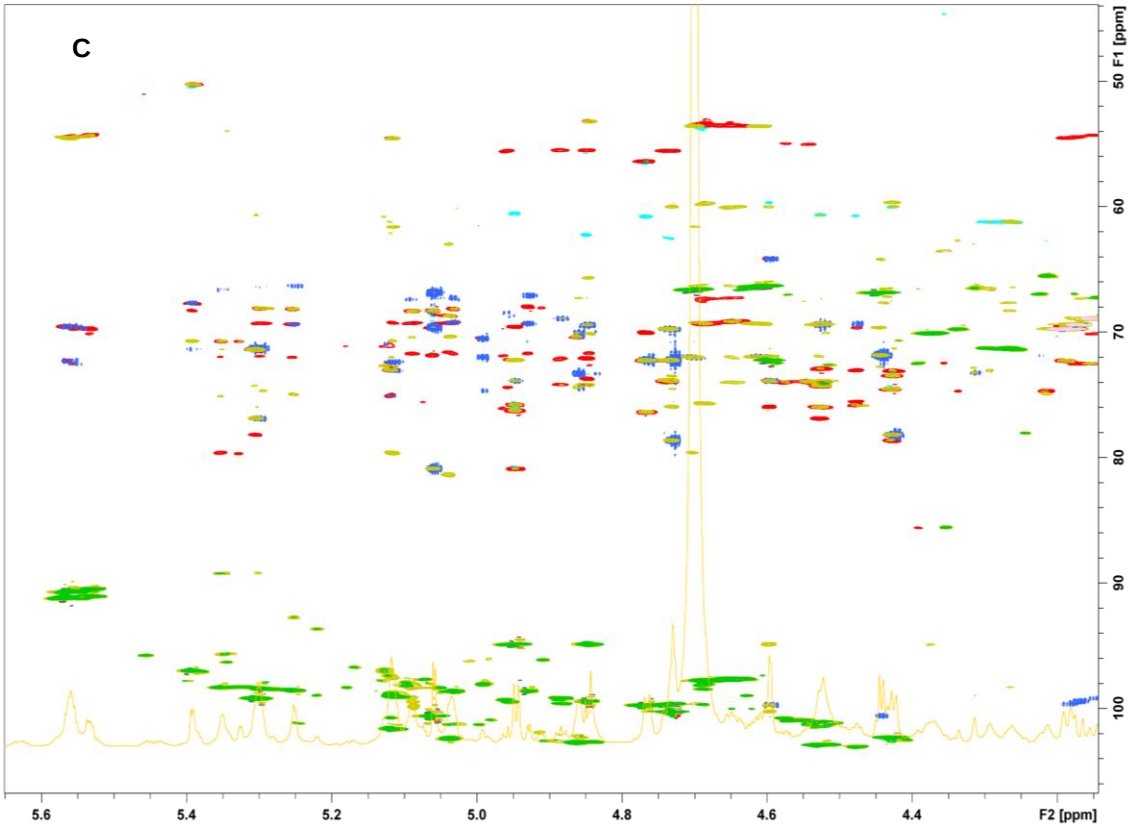

Figure S3 A) ^{1}H NMR spectra and B) zoom in the anomeric region of **OS (OS$_{1deAc}$** and **OS$_{2deAc}$)**, 1.2 GHz; C) HSQC, HSQC-TOCSY (with multiplicity editing), HSQC-NOESY, and HMBC NMR spectra of **OS**, 1.2 GHz. (Abbreviations used: OS = oligosaccharide)

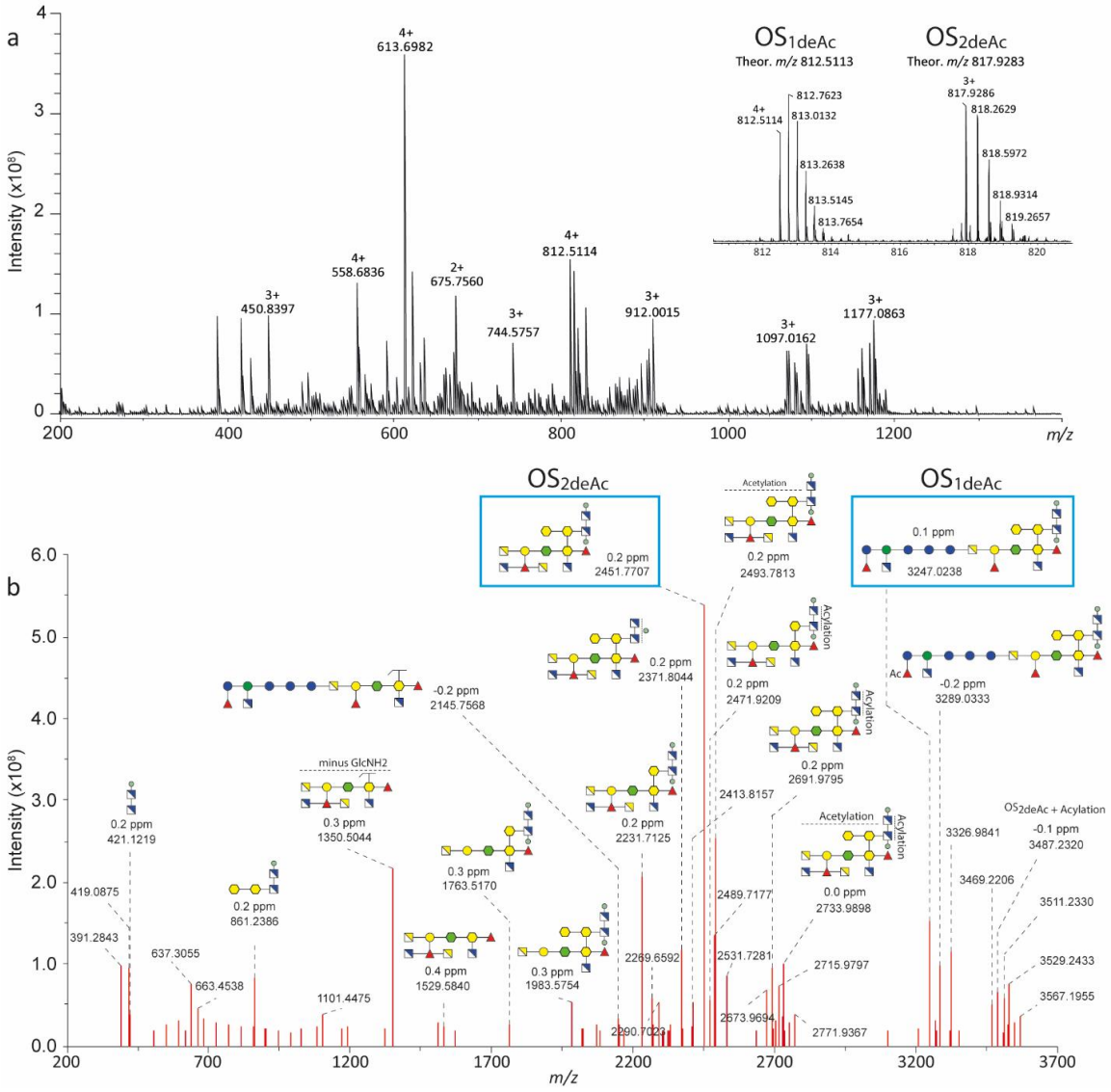

Figure S4. **a)** High-resolution ESI FT-ICR mass spectrum of deacylated LOS. Examples of detected multiply charged and isotopically resolved **OS$_{1deAc}$** and **OS$_{2deAc}$** ion species are depicted in the inset. **b)** Deconvoluted ESI FT-ICR mass spectrum of deacylated LOS. The m/z-values of the monoisotopic peaks of ion species with a relative intensity higher than 3% are reported. Mass measurement errors are indicated in parts per million (ppm). (Abbreviations used: LOS = lipooligosaccharide)

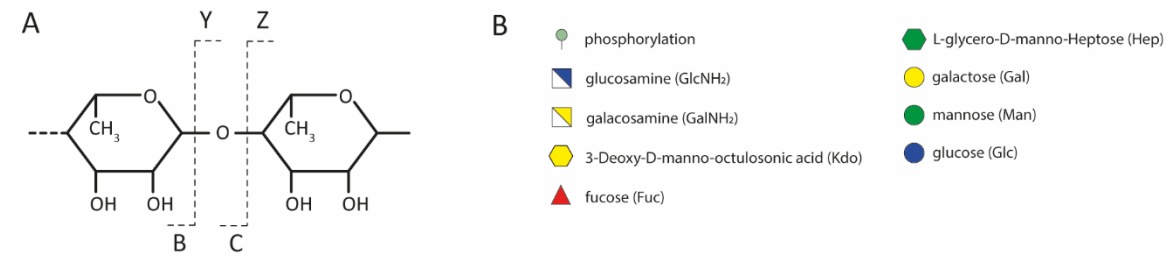

Figure S5. **A)** Fragmentation scheme of the glycosidic bond in collision-induced dissociation of oligosaccharides. **B)** Symbols of monosaccharide residues.

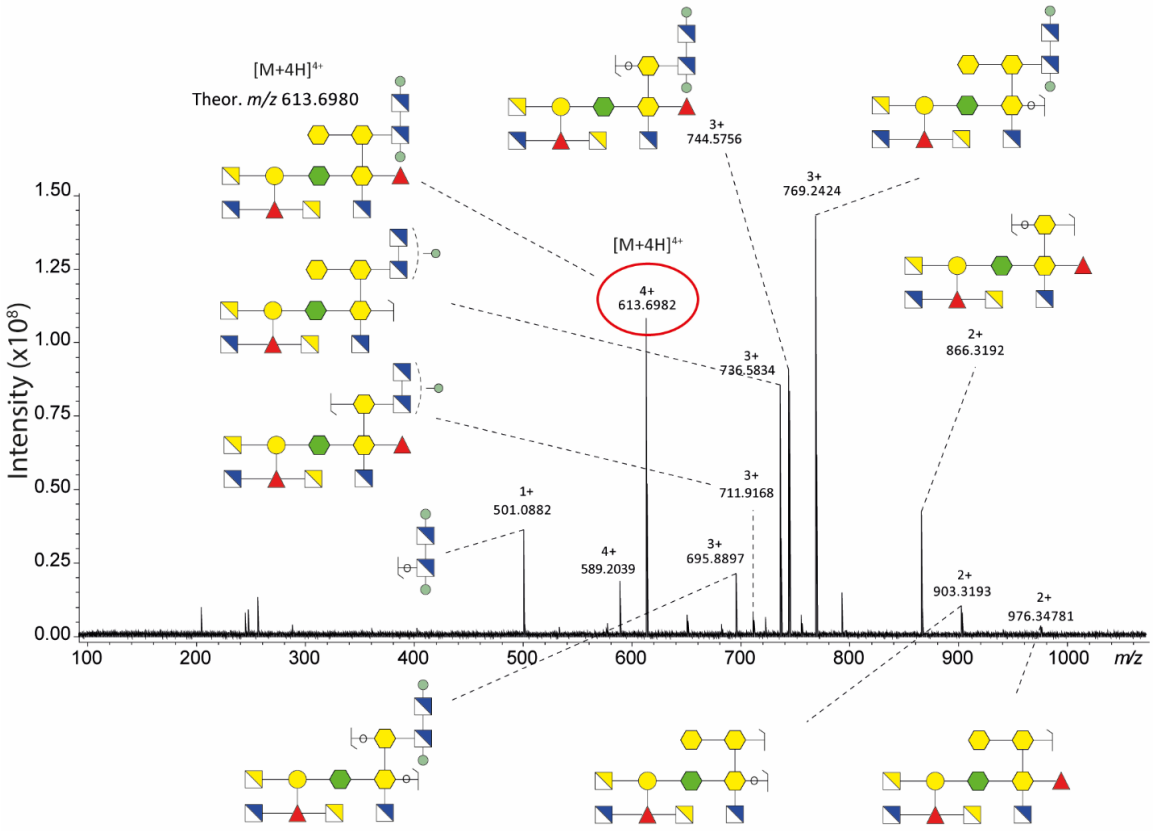

Figure S6. ESI-CID FT-ICR mass spectrum of **OS_{2deAc}** $[M+4H]^{4+}$ detected at m/z 613.6982 (see Fig. S3a), and at m/z 2451.7707 in the deconvoluted mass spectrum (see Fig. S3b). The precursor ion was fragmented with a collision energy of 3 V.

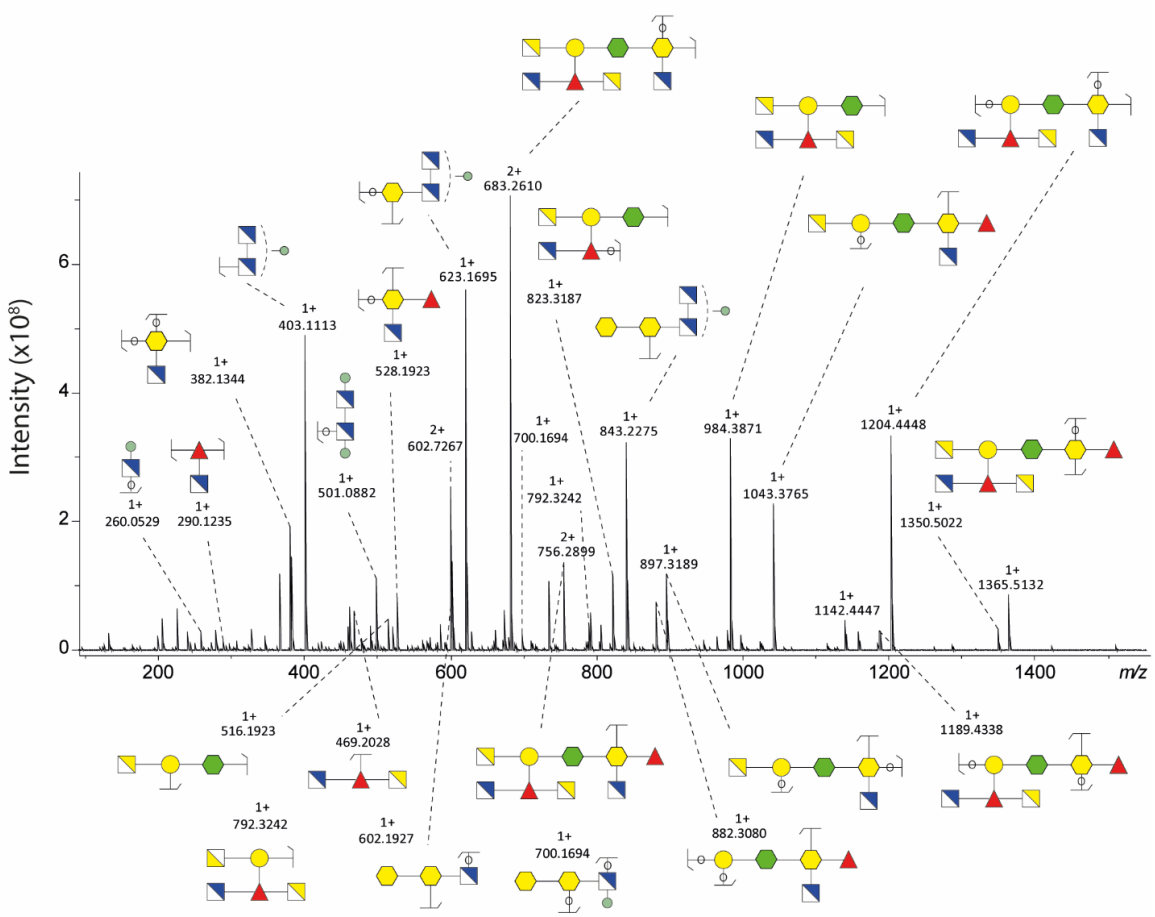

Figure S7. ESI-CID FT-ICR mass spectrum of **OS$_{2deAc}$** $[M+4H]^{4+}$ detected at m/z 613.6982 (see Fig. S3a), and at m/z 2231.7125 in the deconvoluted mass spectrum (see Fig. S3b). The precursor ion was fragmented with a collision energy of 15 V.

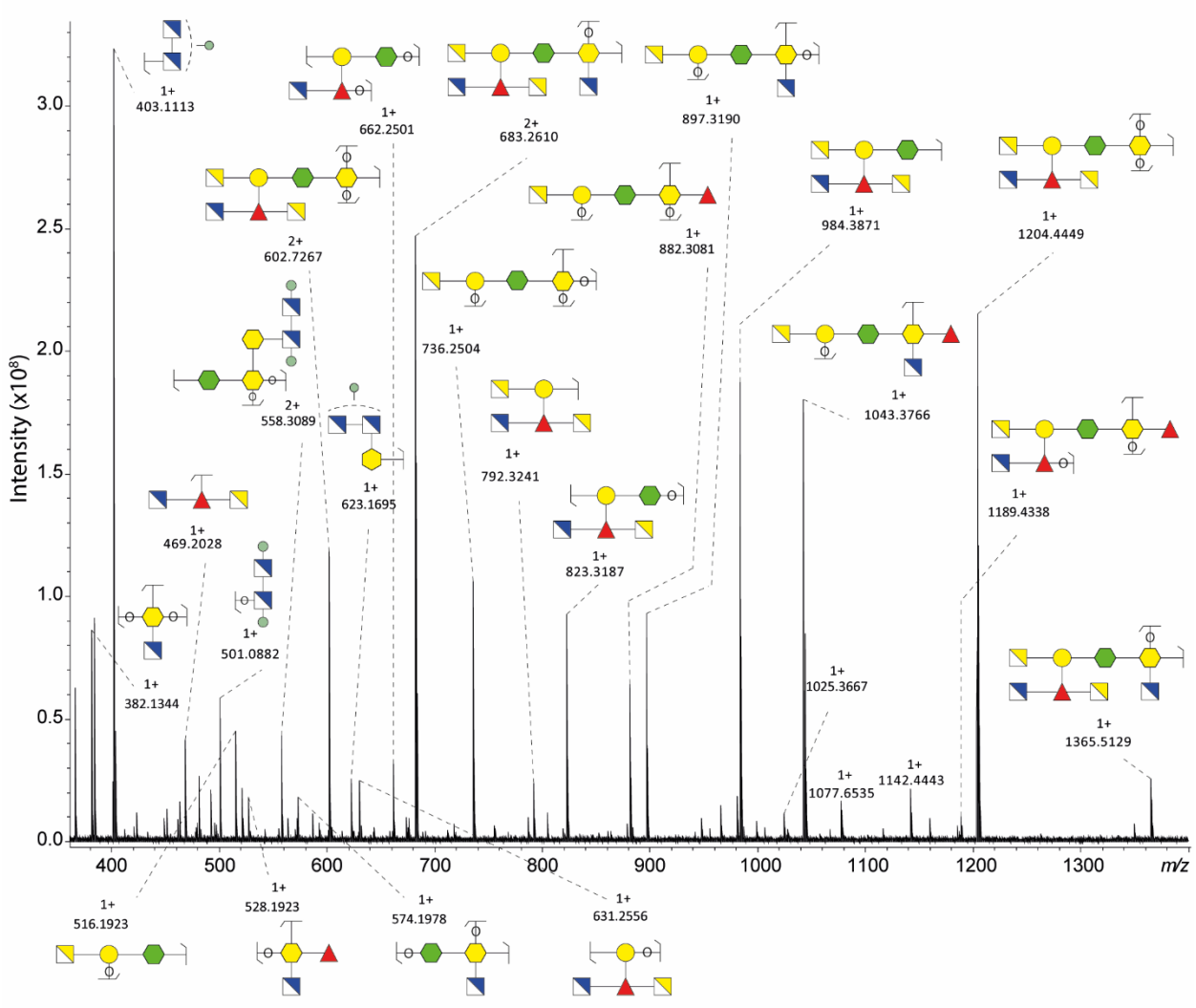

Figure S8. ESI-CID FT-ICR mass spectrum of truncated **OS$_{2deAc}$** $[M+4H]^{4+}$ detected at *m/z* 558.6836 (see Fig. S3a), and at *m/z* 2451.7707 in the deconvoluted mass spectrum (see Fig. S3b).

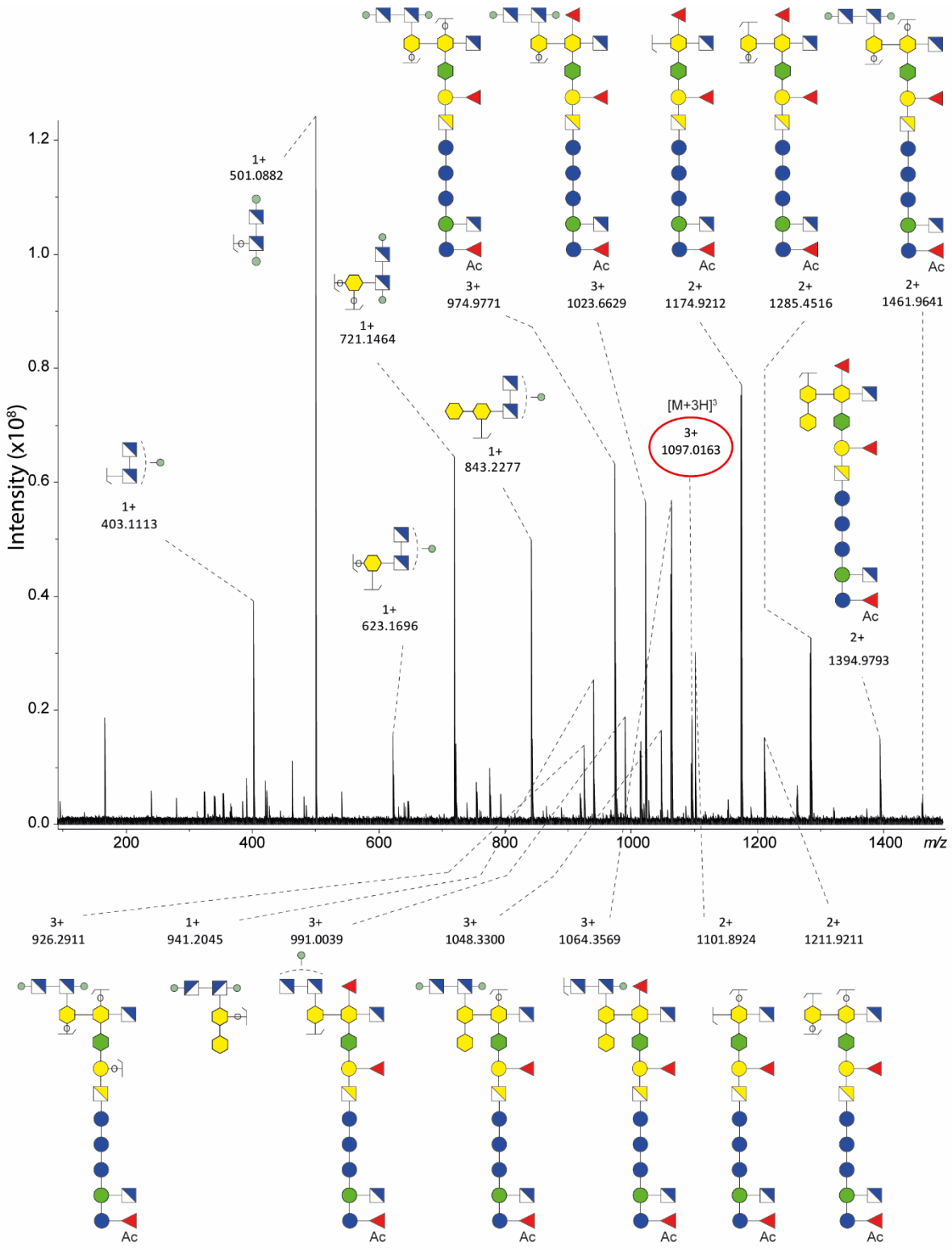

Figure S9. ESI-CID FT-ICR mass spectrum of acetylated **OS$_{1deAc}$** $[M+3H]^{3+}$ detected at *m/z* 1097.0163 (see Fig. S3a), and at *m/z* 3289.03333 in the deconvoluted mass spectrum (see Fig. S3b).

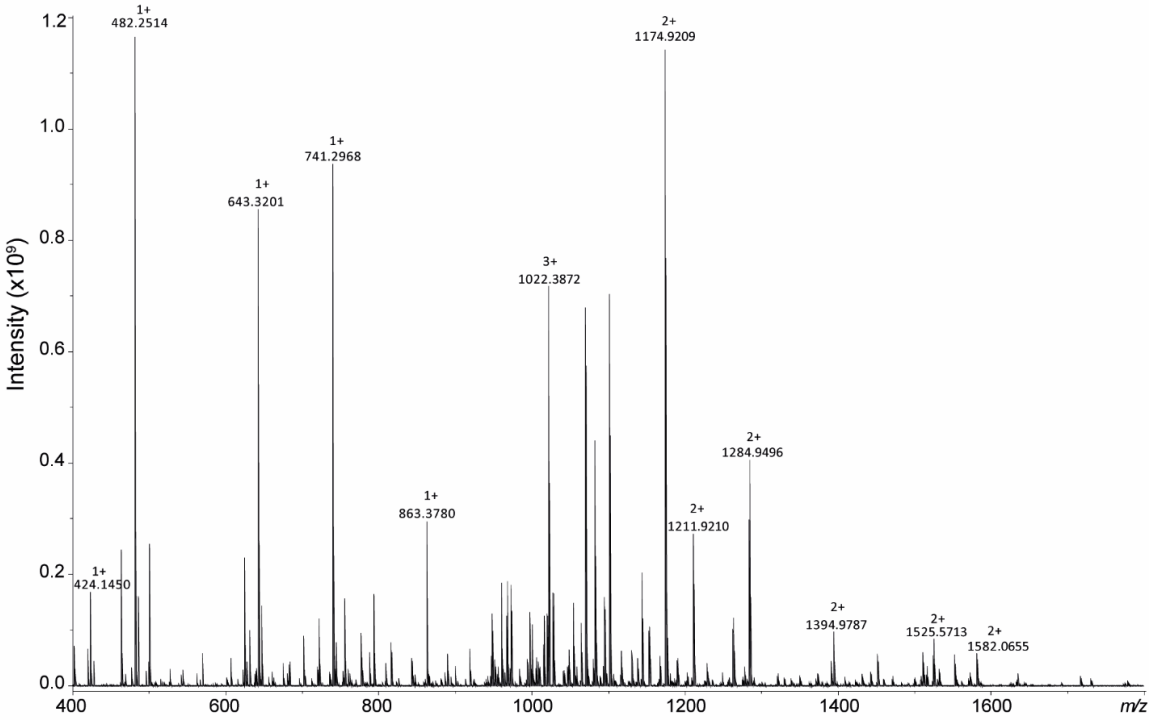

Figure S10. ESI-CID FT-ICR mass spectrum of acetylated and acylated **OS$_{\mathbf{1deAc}}$** $[M+3H]^{3+}$ detected at *m/z* 1177.0863 (see Fig. S3a), and at *m/z* 3529.2433 in the deconvoluted mass spectrum (see Fig. S3b). Assignments in enlarged mass ranges are reported in Figs. S10-S13.

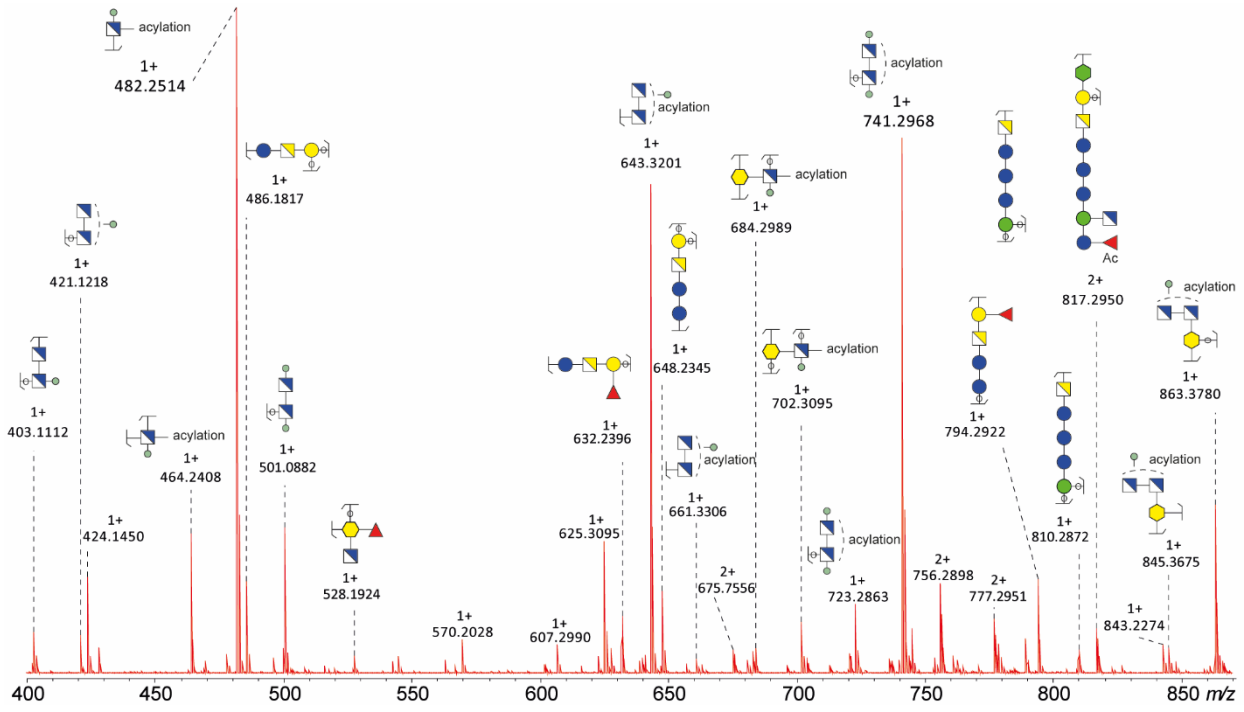

Fig. S11. ESI-CID FT-ICR mass spectrum of acetylated and acylated **OS$_{1deAc}$** $[M+3H]^{3+}$ detected at *m/z* 1177.0863, *m/z* range 400-870. See also Fig. S9 and Figs. S11-S13.

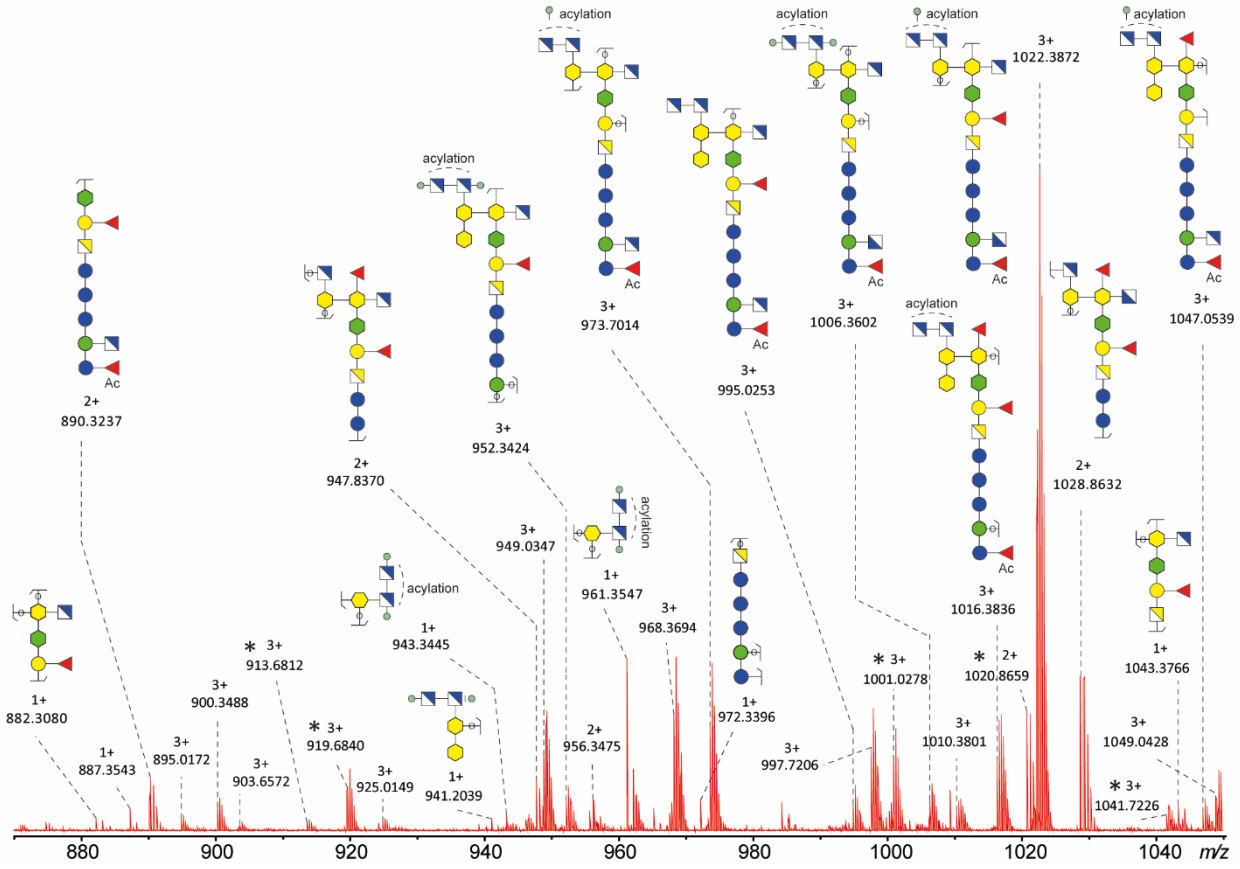

Figure S12. ESI-CID FT-ICR mass spectrum of acetylated and acylated **OS$_{1deAc}$** $[M+3H]^{3+}$ detected at *m/z* 1177.0863, *m/z* range 870-1050. See also Figs. S9-S10 and Figs. S12-S13. * Fragment ions compatible with the simultaneous loss of one fucose and one hexose residue, indicating a potential migration of the acetylated fucose residue.

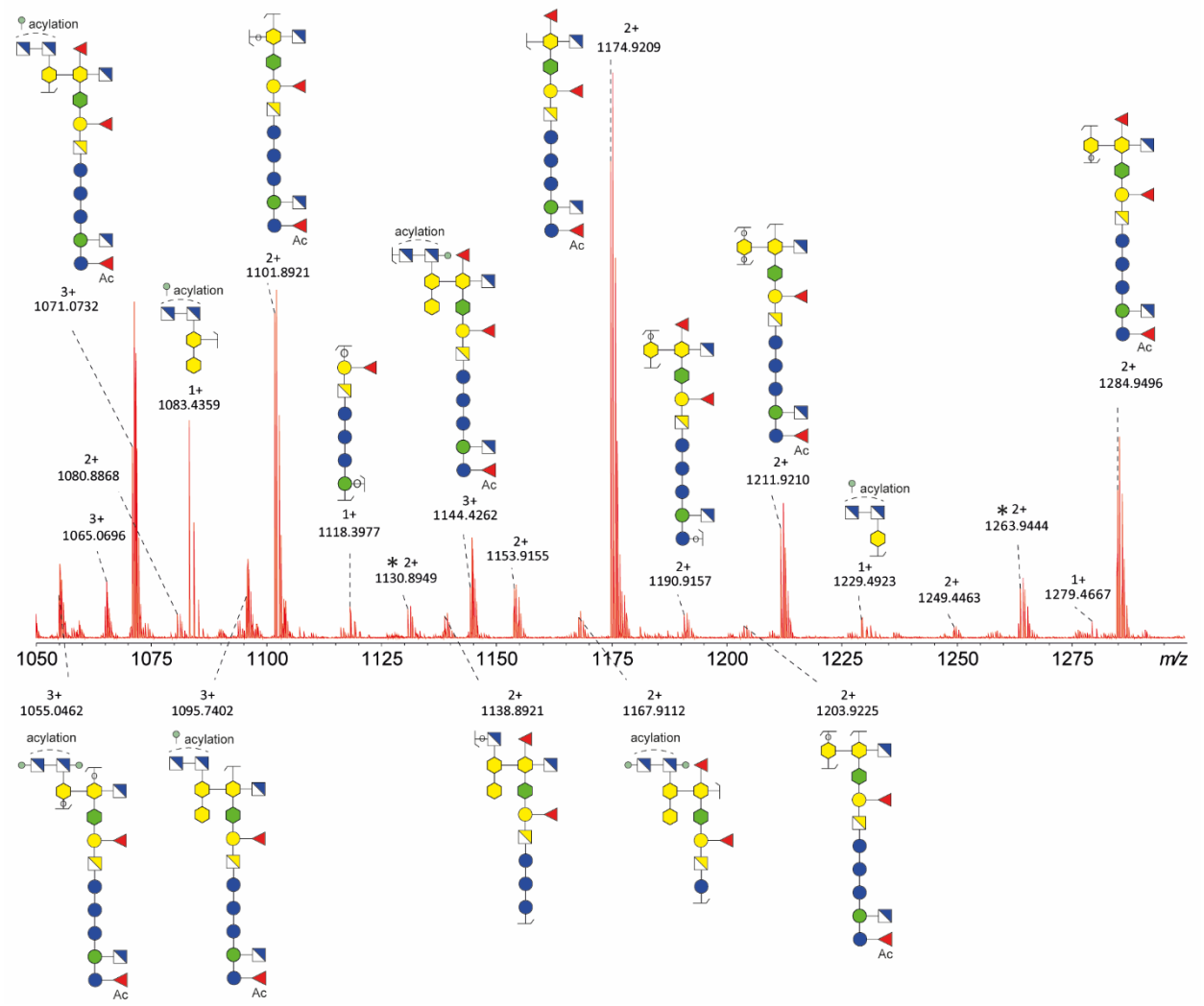

Fig. S13. ESI-CID FT-ICR mass spectrum of acetylated and acylated **OS$_{1deAc}$** $[M+3H]^{3+}$ detected at *m/z* 1177.0863, *m/z* range 1050-1300. See also Figs. S9-S11 and Figs. S13. * Fragment ions compatible with the simultaneous loss of one fucose and one hexose residue, indicating a potential migration of the acetylated fucose residue.

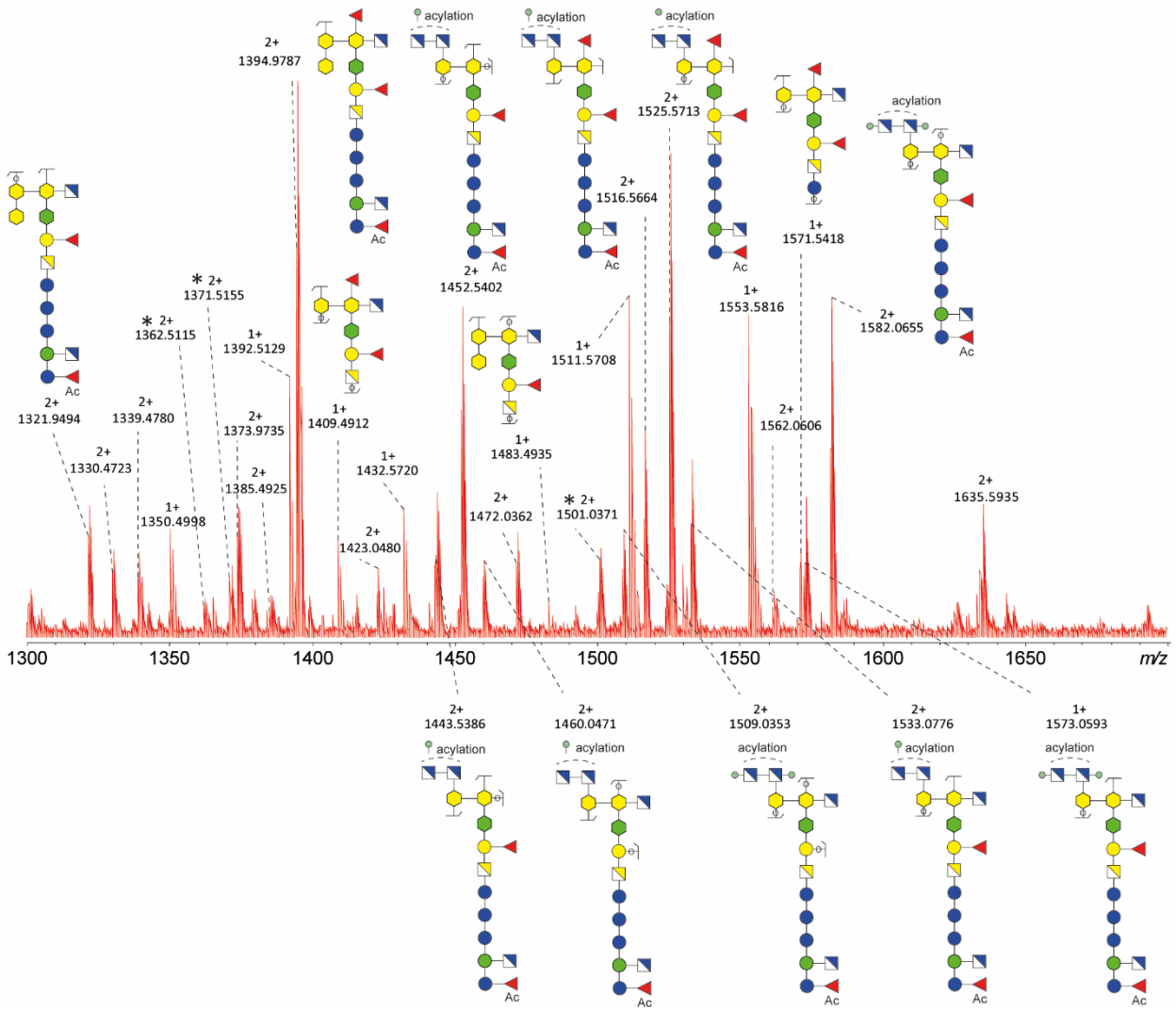

Figure S14. ESI-CID FT-ICR mass spectrum of acetylated and acylated **OS$_{1deAc}$** $[M+3H]^{3+}$ detected at *m/z* 1177.0863, *m/z* range 1300-1700. See also Figs. S9-S12. * Fragment ions compatible with the simultaneous loss of one fucose and one hexose residue, indicating a potential migration of the acetylated fucose residue.

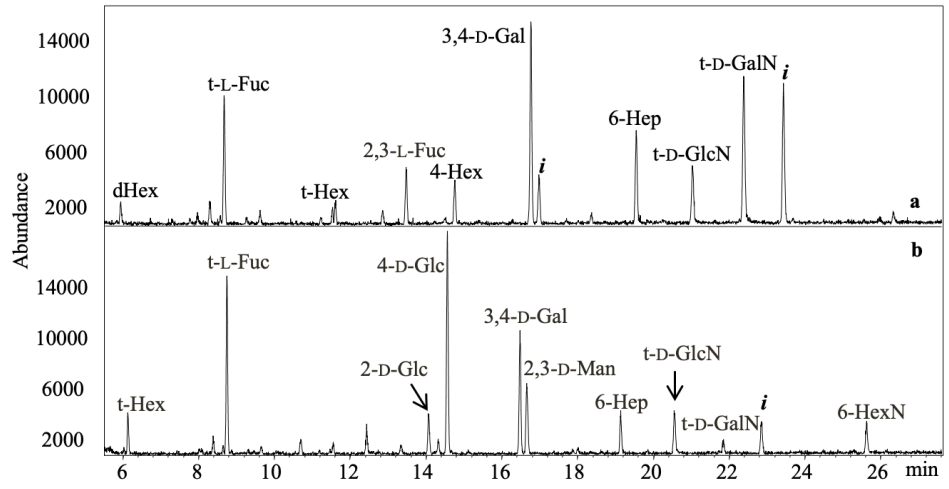

Fig. S15. Methylation analysis of nonasaccharide (OS_2, upper panel a) and tetradecasaccharide (OS_1, bottom panel b) fractions obtained by purification by HPLC.

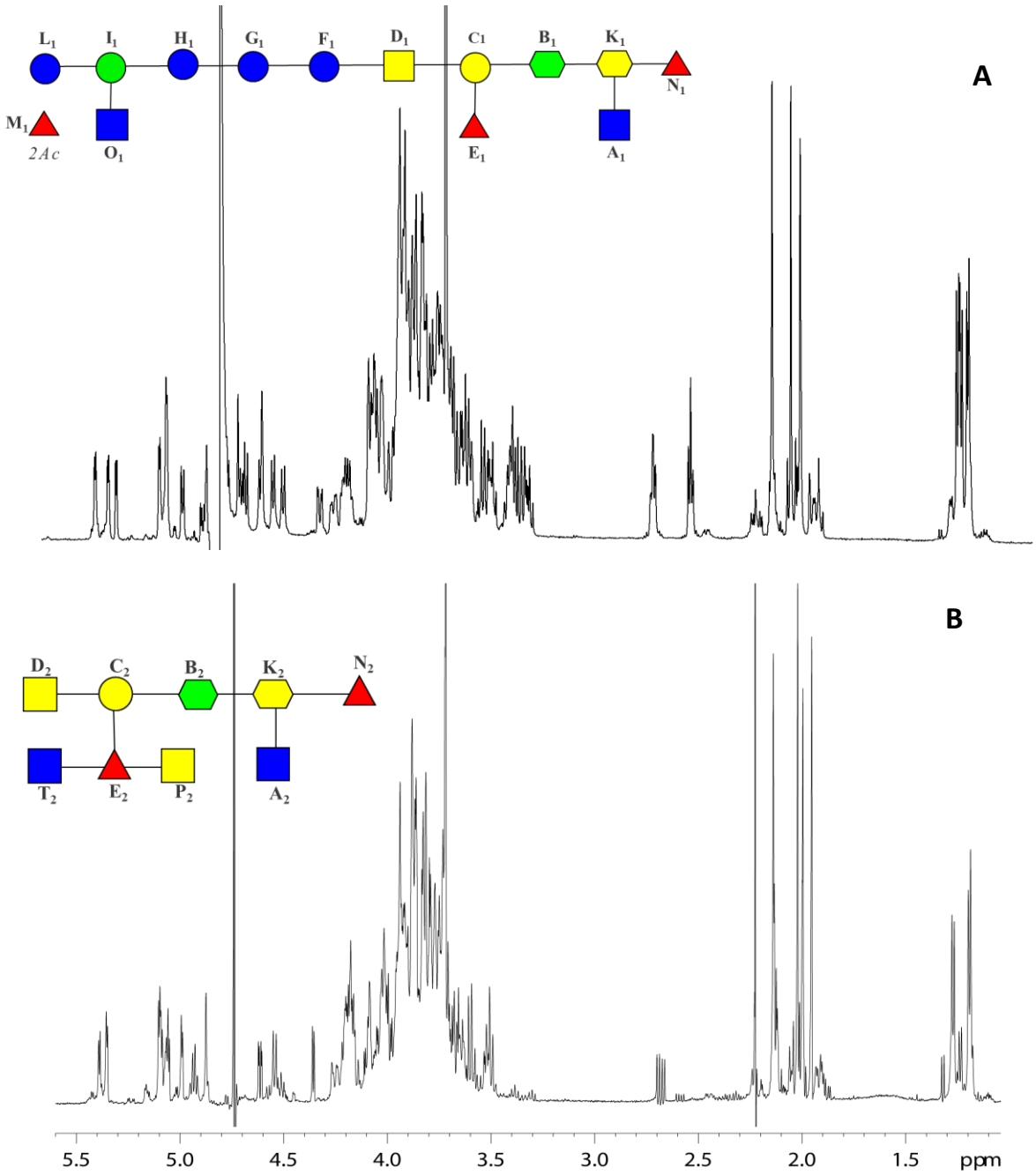

Fig. S16. ^{1}H NMR of the two main fractions obtained by HPLC purification of the oligosaccharide mixture resulting from the acid hydrolysis of *A. muciniphila* Muc^{T} LOS. The fraction were identified as tetradecasaccharide (**OS$_1$**) and as nonasaccharide (**OS$_2$**). The anomeric configuration of each monosaccharide unit was determined based on the $^{3}J_{H1,H2}$ coupling constant values, whereas those of vicinal $^{3}J_{H,H}$ ring coupling constants led to the identification of the relative configuration of each sugar residue. Finally, combined information derived from *inter*-residue NOE connectivity and heteronuclear long-range correlations, together with compositional analysis, allowed the complete characterization of both oligosaccharides.

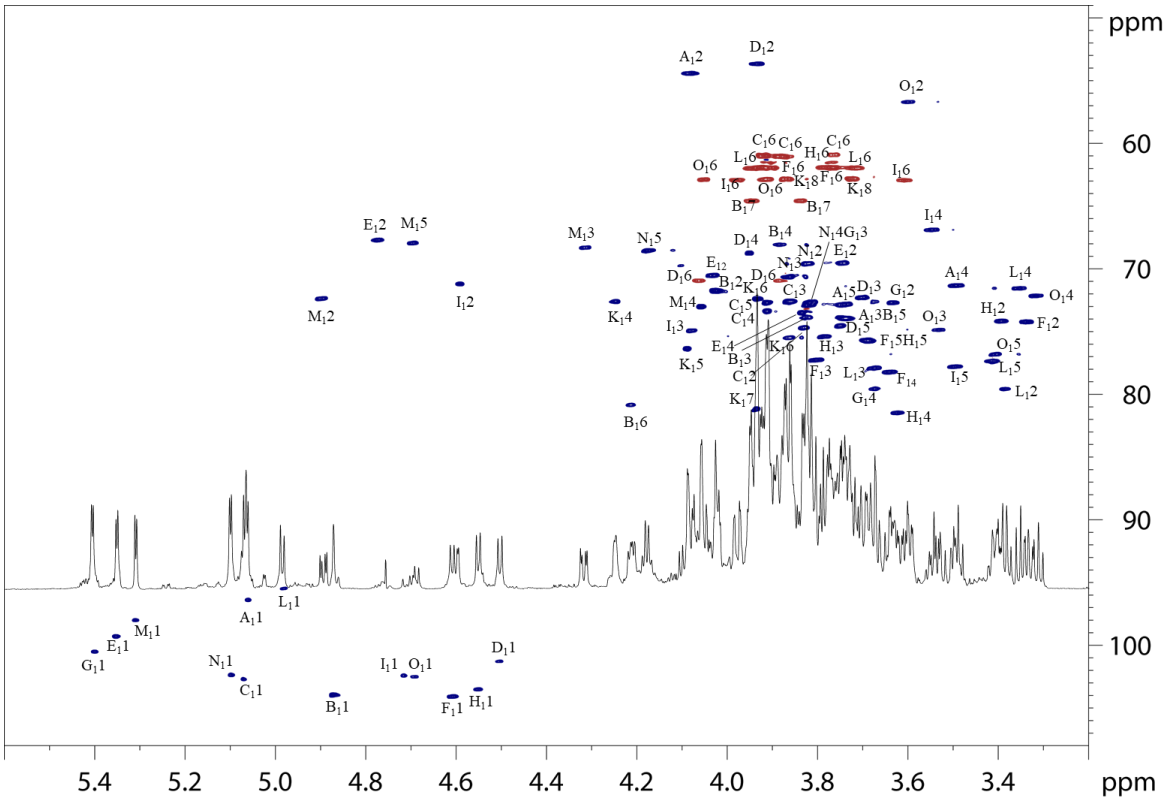

Fig. S17. Zoom of multiplicity edited HSQC spectrum (in red methylene groups, in blue methyne and methyl groups) of **OS1** from *A. muciniphila* Muc^T (950 MHz, 27 °C). Labels refer to table S1.

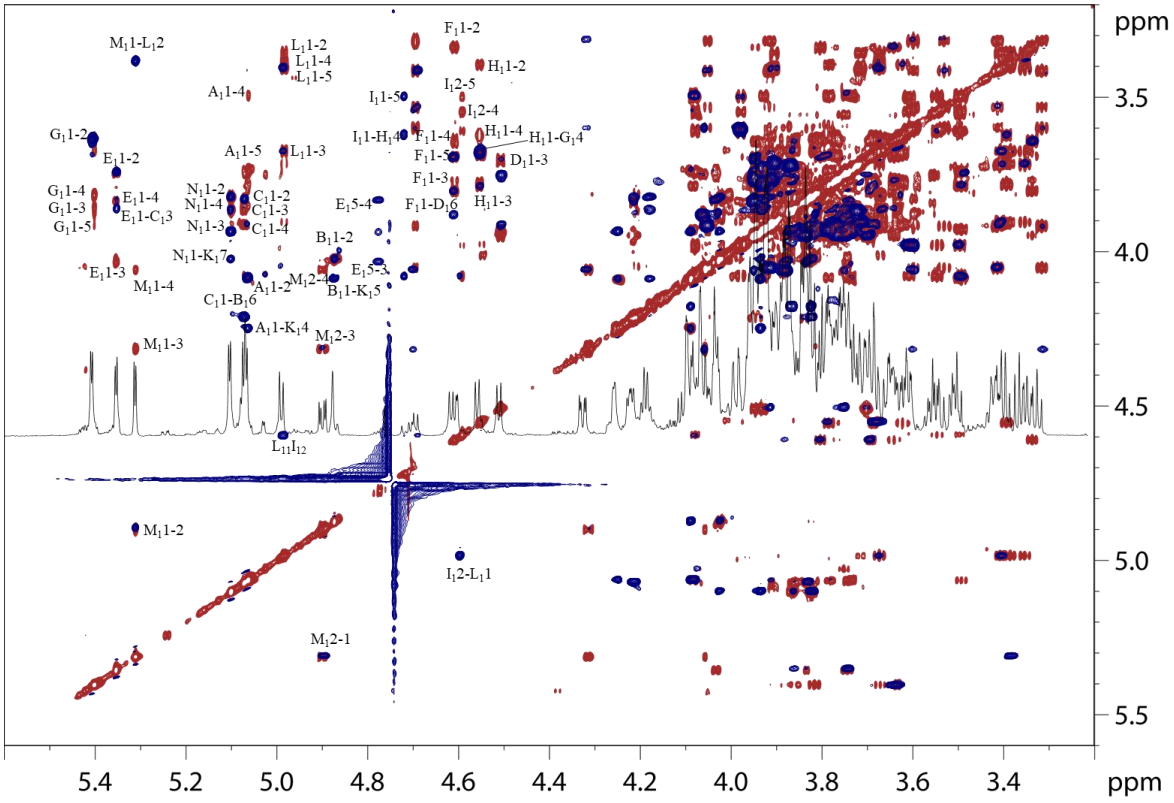

Fig. S18. Expansion of TOCSY (red) and ROESY (blue) spectra of **OS1** from *A. muciniphila* Muc^T (950 MHz, 27 °C). Labels refer to table S1.

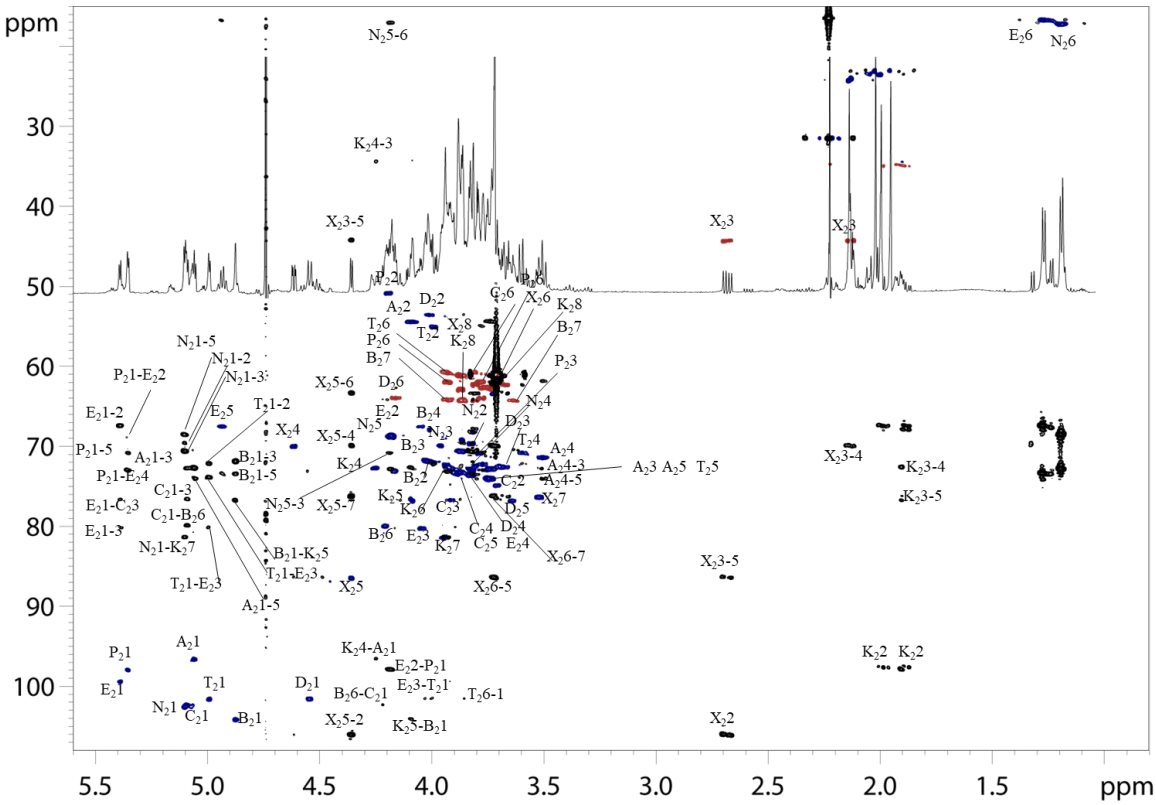

Fig.S19. Zoom of multiplicity edited HSQC spectrum (in red methylene groups, in blue methyne and methyl groups) and HMBC (black) spectrum recorded for **OS_2** from *A. muciniphila* Muc^T (600 MHz, 32 °C). Red densities correspond to "CH_2" carbons. Labels refer to table S2.

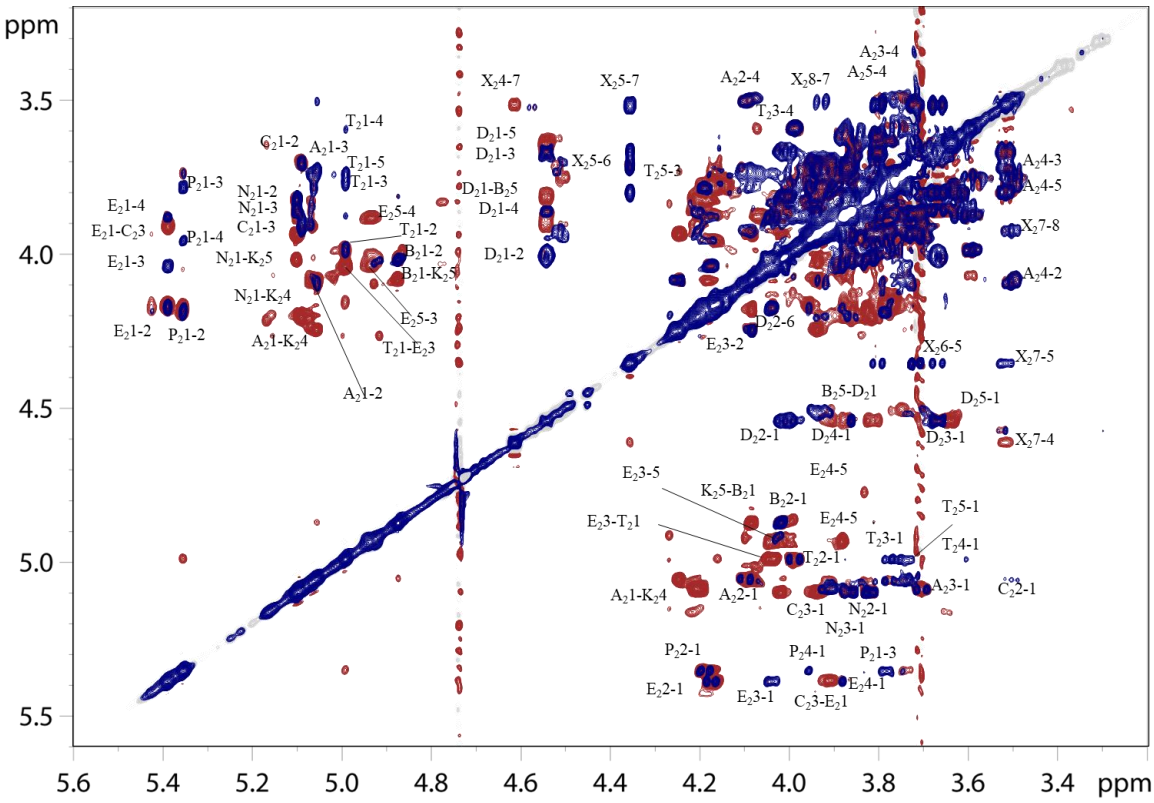

Fig. S20. Expansion of TOCSY (blue) and ROESY (red) spectra of the **OS2** from *A. muciniphila* Muc^{T} (600 MHz, 32 °C). Labels refer to Table S2.

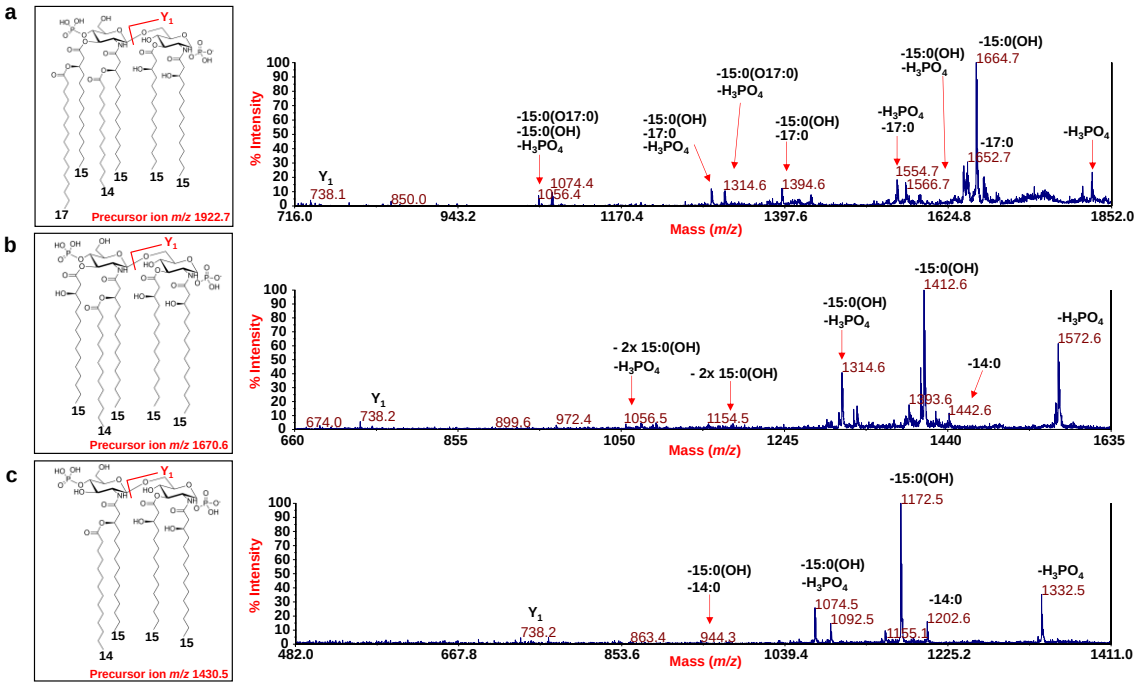

Fig. S21. Negative ion MS/MS spectra of precursor ions at *m/z* 1922.6, *m/z* 1670.6, and *m/z* 1430.6, chosen as representative ion peaks of the clusters matching with *bis*-phosphorylated hexa-, penta-, and tetra-acylated lipid A species from *A. muciniphila* Muc^{T}. The main fragments' assignment is indicated in the spectra. The proposed structures is reported in each inset.

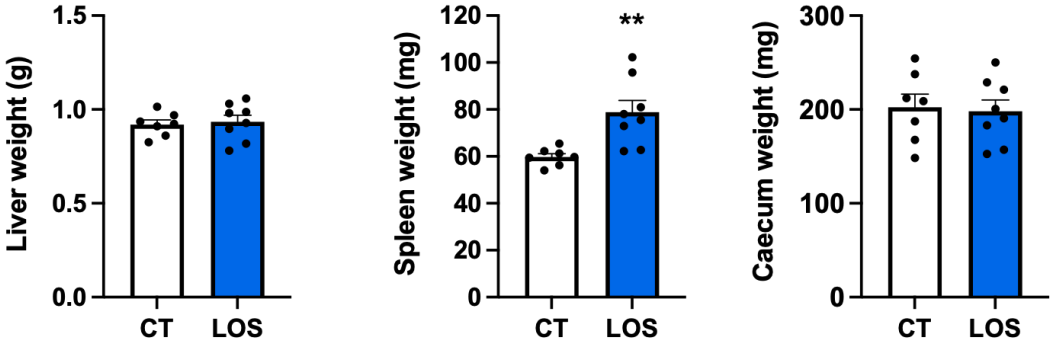

Fig. S22. Weight of the various organs of the mice after intraperitoneal injection of LOS (lipooligosaccharide). Only a small increase in spleen weight was observed. Two groups of mice were injected interperitoneally with 230 µl of LOS solution (generating a final

concentration of 300 µg/kg body weight; LOS group, n = 8) or control (CT; 50 mM Tris-NaCl buffer pH 7; CT group, n = 7). Data are expressed as mean ± SEM and and compared using two-tailed Mann Whitney test (** p-value < 0.005). Source data are provided in the Source Data file.

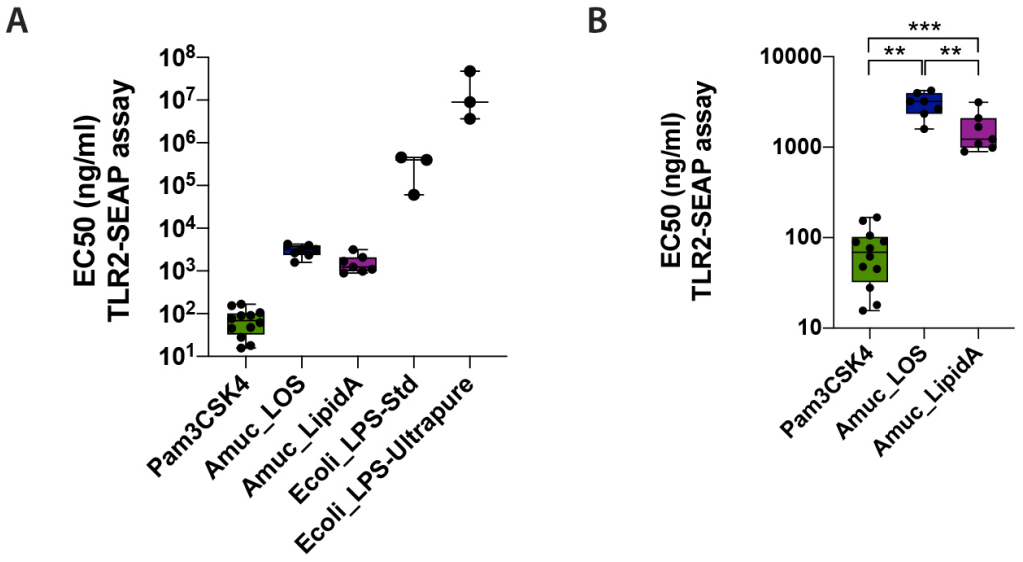

Fig. S23. EC50 of *E. coli* LPS and *A. muciniphila* LOS and LipidA on TLR2. *In vitro* evaluation of potency of *E. coli* LPS (from 2 different sources, with different purity) and *A. muciniphila* LOS and Lipid A on TLR2-expressing cell lines, showcases that the *A. muciniphila* are more potent than *E. coli* LPS (A), with *A. muciniphila* LipidA significantly more potent (i.e. lower EC50) than its LOS (B). Source data are provided in the Source Data file. (Abbreviations used: LPS = lipopolysaccharide, LOS = lipooligosaccharide, TLR = human Toll-Like Receptor, TLR2 = TLR2 expressing cell line also harboring TLR1 and TLR6, SEAP = Secreted Extracellular Alkaline Phosphatase, cf. M&M)

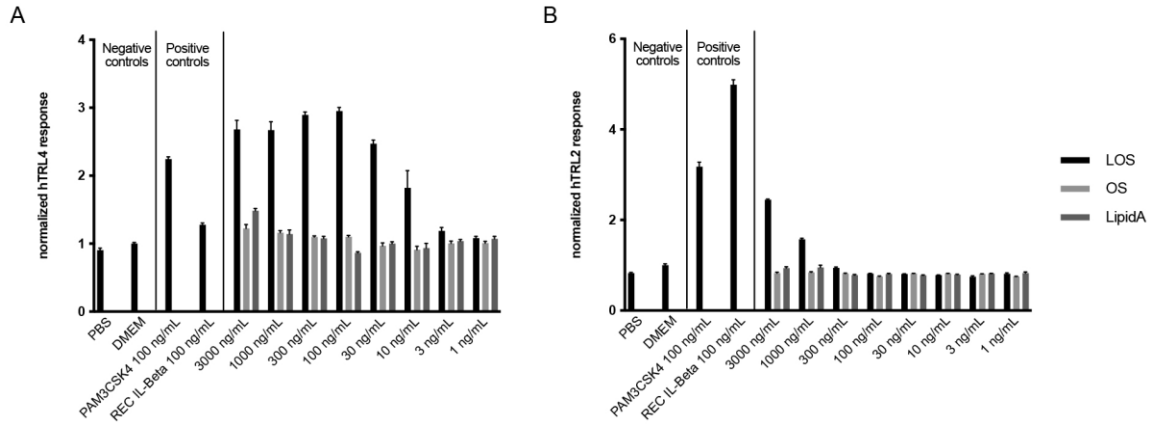

Fig. S24. Activation of TLR4 and TLR2 by *A. muciniphila* and its structural components. The signaling capacity of *A. muciniphila* LOS, OS and lipid A was evaluated by incubating them in HEK-Blue reporter cell lines, expressing hTLR4 (A) and hTLR2 (B). All experiments were performed at least in three biological replicates and representative experiments of three technical replicates with mean +- SD are shown. PBS and DMEM (the culture medium of the cells) were used as negative controls, whilst PAM3CSK4 and REC Il-Beta were used as positive controls as they are known agonists of the cell lines and SEAP system. (Abbreviations used: LOS = lipooligosaccharide, OS = oligosaccharide, hTLR = human Toll-Like Receptor, TLR2 = TLR2 expressing cell line also harboring TLR1 and TLR6). Source data are provided as a Source Data file, and more details are recorded in the Methods section.

Supplementary Tables

Table S1. Proton (^{1}H) and carbon (^{13}C) NMR chemical shifts of the fully deacylated lipooligosaccharide **OS** (composed of OS_{1deAc} and OS_{2deAc}) from *A. muciniphila* Muc^{T} (1.2 GHz, 25 °C, D_2O).

	1	**2**	**3**	**4**	**5**	**6**	**7**	**8**
D_1 6-β-GalN	4.65	2.98	3.79	3.87	3.76	3.94/3.63		
	97.63	53.5	69.3	67.3	74.0	69.34		
E_1 t-α-Fuc	5.30/5.25	3.68/3.67	3.70	3.86/3.84	4.603	1.09		
	98.4/98.6	68.2	69.3	71.9	66.3	15.3		
F_1 4-β-Glc	4.52	3.23	3.70	3.54	3.62	3.66/3.84		
	102.83	72.9	75.9	76.8	74.18	60.6		
G_1 4-α-Glc	5.304	3.52	3.71	3.55	3.76	3.809/3.76		
	99.16	71.2	71.2	78.14	72.05	59.68		
H_1 4-β-Glc	4.42	3.27	3.72	3.63	3.58	3.80/3.65		
	102.27	73.08	73.49	78.63	74.9	59.93		
I_1 2-β-Man	4.72	4.596	4.06	3.73	3.38	3.80/3.76		
	100.23	72.2	73.87	64.12	75.96	59.64		
L_1 2,3-β-Glc	4.945	3.33	3.64	3.35	3.35	3.83/3.64		
	94.8	80.855	76.23	69.53	75.77	60.54		
M_1 t-α-Fuc	5.06	3.72	3.81	3.929	4.42	1.128		
	100.57	71.8	69.6	71.8	66.85	15.48		
O_1 t-β-GlcN	4.76	2.62	3.64	3.25	3.37	3.91/3.74		
	99.71	56.37	72.3	70.02	76.37	60.75		
P_2 **t-α–GalN**	5.388	3.29	3.78	3.91	3.70			
	96.9	50.2	67.65	68.3	71.3			
E_2 2,3-α-Fuc	5.35/5.32	4.02/4.01	3.94	3.87	4.077	1.13		
	99.4	70.6	79.65	71.9	66.6	16.3		
T_2 t-α-GlcN	5.11	2.90	3.63	3.43	3.66	3.70/3.75		
	101.5	54.46	73.1	69.2	72.3	59.8		
D_2 t-β-GalN	4.64	2.79	3.79	3.87	4.07	3.74		
	97.74	53.5	69.3	67.3	72.0	60.77		
Residue common to the two oligoes (almost isochronous)								
$A_{1/2}$ t-α-GlcN	4.88/ 4.95	2.94						
	99.4	55.39						
$B_{1/2}$ 6-α-Hep	4.85	3.99	3.86			3.94 / 4.02	3.91/3.81	
	102.67	70.3	69.65			79.6	63.3	
$K_{1/2}$ 4,5,7-α-Kdo	----	----	1.66/1.96	3.96	3.88		3.958	4.03/3.95
	174	99.4	34.395	72.0	73.21		81.3	63.0
$C_{1/2}$ 3,4-α-Gal	5.11 / 5.128	3.74 / 3.76	3.84/3.87	4.01/3.99	3.67	3.85		
	101.0	72.2 / 72.1	74.9/74.7	70.3/70.7	68.2	60.5		
$N_{1/2}$ t-α-Fuc	5.03	3.69	3.71	3.99	4.09	1.14/1.12		
	102.3	68.09	69.19	70.3	67.37	15.6		
Lipid A Skeleton								
6–α-GlcN	5.56	3.34/ 3.30/ 3.28/ 3.36	3.80	3.65	4.05	4.18/363		
	90.98/9.67/90.51	54.4	69.66	69.4	72.3	69.7		
6-β-GlcN	4.73	2.94	3.74	3.65	3.62	3.29/3.59		
	99.64	55.5	72.12	72.12	74.06	62.4		

Table S2. Proton (^{1}H) (plain text) and carbon (^{13}C) (*italic*) NMR chemical shifts of **OS1** from *A. muciniphila* Muc^{T} (950 MHz, 27 °C, D_2O).

	1	**2**	**3**	**4**	**5**	**6**	**7**	**8**
A_1 t-α-GlcNAc	5.06	4.08	3.73	3.48	3.74	3.77/3.93		
	96.6	*54.4*	*73.9*	*71.3*	*72.8*	*61.9*		
	$^{1}J_{CH}$= 170.2 Hz	*N-acetyl 2.13 / 24.1 and 175.0 ppm*						
B_1 6-α-Hep	4.87	4.02	3.83	3.88	3.74	4.21	3.94/3.83	
	104.1	*71.7*	*73.8*	*68.1*	*73.8*	*80.8*	*64.5*	
	$^{1}J_{CH}$= 169.0 Hz							
C_1 3,4-α-Gal	5.97	3.83	3.86	3.91	3.91	3.77/3.92		
	102.7	*74.7*	*72.6*	*73.3*	*72.7*	*60.8*		
	$^{1}J_{CH}$= 169.5 Hz							
D_1 6-β-GalNAc	4.50	3.93	3.71	3.95	3.75	3.86/4.07		
	101.3	*53.6*	*72.4*	*68.6*	*74.5*	*70.9*		
	$^{1}J_{CH}$= 166.1Hz	*N-acetyl 2.00 / 23.4 and 175.3 ppm*						
E_1 t-α-Fuc	5.35	3.74	4.03	3.83	4.77	1.23		
	99.3	*69.5*	*70.5*	*73.5*	*67.8*	*16.7*		
	$^{1}J_{CH}$= 173.9 Hz							
F_1 4-β-Glc	4.61	3.34	3.80	3.64	3.69	3.77/3.95		
	103.9	*74.2*	*77.3*	*78.3*	*75.7*	*61.9*		
	$^{1}J_{CH}$=162.3 Hz							
G_1 4-α-Glc	5.40	3.63	3.81	3.67	3.86	3.88		
	100.5	*72.7*	*72.7*	*79.56*	*72.6*	*61.1*		
	$^{1}J_{CH}$= 172.5 Hz							
H_1 4-β-Glc	4.55	3.39	3.78	3.62	3.68	3.77/3.91		
	103.6	*74.15*	*75.4*	*81.0*	*75.7*	*61.4*		
	$^{1}J_{CH}$=163.7 Hz							
I_1 2-β-Man	4.71	4.59	4.07	3.55	3.49	3.61/3.97		
	102.5	*71.2*	*74.8*	*66.9*	*77.8*	*62.87*		
	$^{1}J_{CH}$=160.5 Hz							
K_1 4,5,7-Kdo			1.90/2.22	4.25	4.09	3.93	3.93	3.87/3.72
	174.7	*97.9*	*34.6*	*72.6*	*76.2*	*72.3*	*81.0*	*62.8*
L_1 2,3-β-Glc	4.98	3.38	3.67	3.35	3.41	3.71/3.91		
	95.5	*79.5*	*77.8*	*71.5*	*77.3*	*61.9*		
	$^{1}J_{CH}$= 164.8 Hz							
M_1 t-α-Fuc	5.31	4.90	4.32	4.06	4.69	1.22		
	98.00	*74.4*	*68.3*	*73.0*	*69.9*	*16.4*		
	$^{1}J_{CH}$=174.5 Hz	*2-O-acetyl 2.12 / 24.1 and 175.0 ppm*						
N_1 t-α-Fuc	5.10	3.81	3.86	3.82	4.17	1.19		
	102.5	*69.5*	*72.5*	*72.9*	*68.5*	*16.97*		
	$^{1}J_{CH}$= 172.3 Hz							
O_1 t-β-GlcNAc	4.69	3.61	3.53	3.31	3.41	4.05/3.91		
	102.5	*54.6*	*74.8*	*72.1*	*76.8*	*63.0*		
	$^{1}J_{CH}$= 162.6 Hz	*N-acetyl 2.05 / 23.4 and 175.4 ppm*						

Table S3. Proton (^{1}H) (plain text) and carbon (^{13}C) (*italic*) NMR chemical shifts of **OS2** from *A. muciniphila* Muc^{T} (600 MHz, 32 °C, D_2O).

	1	**2**	**3**	**4**	**5**	**6**	**7**	**8**
K₂ 4,5,7-Kdo*p*			1.89/1.98	4.25	4.09	3.94	3.94	3.87/3.76
	175.9	*97.75*	*34.96*	*72.6*	*76.6*	*72.4*	*81.5*	*62.7*
A₂ t-α-GlcNAc	5.06	4.10	3.72	3.50	3.74			
	96.8	*54.4*	*72.7*	*71.4*	*73.9*			
	$^{1}J_{CH}$= 171.3 Hz	*N-acetyl 2.14 / 24.2 and 175.4 ppm*						
B₂ 6-α-Hep	4.87	4.03	4.03	4.01	3.82	4.21	3.62/3.92	
	104.1	*71.7*	*71.7*	*68.0*	*73.6*	*79.9*	*64.2*	
	$^{1}J_{CH}$=167.5 Hz							
C₂ 3,4-α-Gal	5.09	3.69	3.91	3.89	3.87	3.82		
	102.9	*74.7*	*76.4*	*72.8*	*72.7*	60.6		
	$^{1}J_{CH}$=170.2 Hz							
D₂ t-β-GalNAc	4.55	4.00	3.66	3.86	3.64	4.16/3.77		
	101.6	*53.4*	*69.2 73.2*	*72.6*	*76.7*	*63.9*		
	$^{1}J_{CH}$= 161.8 Hz	*N-acetyl 2.04 / 23.5 and 175.3 ppm*						
E₂ 2,3-α-Fuc	5.39	4.18	4.05	3.88	4.93	1.27		
	99.4	*68.6*	*80.2*	*73.2*	*67.2*	*16.3*		
	$^{1}J_{CH}$= 175.8 Hz							
T₂ t-α-GlcNAc	4.99	3.99	3.79	3.59	3.74	3.86		
	101.8	*55.2*	*72.3*	*70.6*	*73.9*	*60.9*		
	$^{1}J_{CH}$= 172.4 Hz	*N-acetyl 1.95 / 23.1 and 174.8 ppm*						
P₂ t-α-GalNAc	5.36	4.20	3.79	3.95	4.17	3.79/3.87		
	97.9	*50.7*	*70.4*	*69.7*	*68.8*	*62.6*		
	$^{1}J_{CH}$= 174.9 Hz	*N-acetyl 2.03 / 23.2 and 175.4 ppm*						
N₂ t-α-Fuc	5.09	3.81	3.86	3.82	4.18	1.27		
	102.9	*69.6*	*70.5*	*72.8*	*68.6*	*16.3*		
	$^{1}J_{CH}$=169.5 Hz							
X₃ Free Kdo*f*			2.13/2.69	4.62	4.37	3.72	3.51	3.77/3.92
		105.6	*44.3*	*70.1*	*86.3*	*63.3*	*76.3*	*61.8*

Table S4. Fatty acid content of the LOS isolated from *A. muciniphila* Muc^T; i= iso a = anteiso

Fatty Acid Composition
12:0; 13:0; i-14:0; *i*-15:0; 15:0; 14:0 (3-OH) ; *i*-16:0; 16:0; *i*-15:0 (3- OH); *i*-17:0; a-17:0; 17:0; 16:0 (3-OH) ; *i*-17:0- (3-OH)

Table S5. The main ion peaks observed in the MALDI-TOF MS spectra reported in Fig. 2, the predicted masses, and the proposed interpretation of the fatty acids and phosphate on the lipid A backbone. The observed masses are compared to the calculated monoisotopic mass (predicted mass, Da) of each ion based on the proposed lipid A structures. For description purposes, the 17:0 acyl moiety has been reported simply as 17:0, taking into consideration that it can be also found in its iso- and anteiso-branched structure, according to compositional analysis

Predicted mass (Da)	**Observed ion peaks (*m*/*z*)**	**Acyl substitution**	**Proposed fatty acid/phosphate composition**
1923.3	1922.6	Hexaacyl	$HexN_2P_2$ [*i*15:0(3-OH)]$_4$ (17:0) (*i*14:0)
1843.3	1842.6	Hexaacyl	$HexN_2P$ [*i*15:0(3-OH)]$_4$ (17:0) (*i*14:0)
1671.1	1670.3	Pentaacyl	$HexN_2P_2$ [*i*15:0(3-OH)]$_4$ (*i*14:0)
1591.1	1590.4	Pentaacyl	$HexN_2P$ [*i*15:0(3-OH)]$_4$ (*i*14:0)
1430.9	1430.1	Tetraacyl	$HexN_2P_2$ [*i*15:0(3-OH)]$_3$ (*i*14:0)
1350.9	1350.1	Tetraacyl	$HexN_2P$ [*i*15:0(3-OH)]$_3$ (*i*14:0)

Table S6. Predicted genes involved in LOS synthesis. The genome of *A. muciniphila* MucT harbors diverse genes and gene clusters that can play a role in LOS biosynthesis, including genes involved in fucose biosynthesis. All genes were found to be expressed at the transcriptional level when *A. muciniphila* MucT was grown on mucus whereas those marked (#) were also detected at the proteome level[20].

Gene number	Function	CAZy family
Amuc_0442#	GT	GT4
Amuc_0474#	CMP-KDO transferase	GT30
Amuc_0634	GT	GT8
Amuc_0659#	1,2-diacylglycerol 3-β-galactosyltransferase	GT28
Amuc_0753	GT	GT8
Amuc_0755#	GlcNAc transferase	GT9
Amuc_0759	GT	GT4
Amuc_0760	Fucosyltransferase	GT10
Amuc_0939	GT	GT8
Amuc_0942#	GDP-L-Fuc: galactoside α-1,2-L-fucosyltransferae	GT11
Amuc_0973	Diacylglycerol galactosyltransferase	GT28
Amuc_1077#	GT	GT4
Amuc_1141#	GDP-L-Fuc: galactoside α-1,2-L-fucosyltransferase	GT11
Amuc_1248#	GDP-Fucose synthetase	-
Amuc_1405#	GT	GT4
Amuc_1869#	GT	GT4
Amuc_2052#	Lipid A disaccharide synthase	GT19
Amuc_2081-Amuc_2094#	EPS/LPS biosynthesis cluster	Cluster rich in GT2 and GT4
Amuc_2092	LpxA like (UDP-N-GlcNAc acyltransferase)	Biosynthesis Lipid A

REFERENCES

1 Derrien, M., Collado, M. C., Ben-Amor, K., Salminen, S. & de Vos, W. M. The Mucin degrader Akkermansia muciniphila is an abundant resident of the human intestinal tract. *Appl Environ Microbiol* **74**, 1646-1648, doi:10.1128/AEM.01226-07 (2008).

2 Galanos, C., Luderitz, O. & Westphal, O. A new method for the extraction of R lipopolysaccharides. *European journal of biochemistry / FEBS* **9**, 245-249, doi:10.1111/j.1432-1033.1969.tb00601.x (1969).

3 Westphal, O. & Jann, K. Bacterial Lipopolysaccharides. Extraction with Phenol-Water and Further Applications of the Procedure. *Methods in Carbohydrate Chemistry* **5**, 83-91 (1965).

4 Hirschfeld, M, Ma Y, Weis, JH, Vogel, SN, Weis, JJ. Cutting edge: repurification of lipopolysaccharide eliminates signaling through both human and murine toll-like receptor 2. *J Immunol.* 165(2), 618-22 (2000), doi: 10.4049/jimmunol.165.2.618

5 Pither, M. D., McClean, S., Silipo, A., Molinaro, A. & Di Lorenzo, F. A chronic strain of the cystic fibrosis pathogen Pandoraea pulmonicola expresses a heterogenous hypo-acylated lipid A. *Glycoconjugate journal* **38**, 135-144, doi:10.1007/s10719-020-09954-8 (2021).

6 Silipo, A., Lanzetta, R., Amoresano, A., Parrilli, M. & Molinaro, A. Ammonium hydroxide hydrolysis: a valuable support in the MALDI-TOF mass spectrometry analysis of Lipid A fatty acid distribution. *J Lipid Res* **43**, 2188-2195, doi:10.1194/jlr.d200021-jlr200 (2002).

7 Haishima, Y., Holst, O. & Brade, H. Structural investigation on the lipopolysaccharide of Escherichia coli rough mutant F653 representing the R3 core type. *European journal of biochemistry / FEBS* **203**, 127-134, doi:10.1111/j.1432-1033.1992.tb19837.x (1992).

8 Holst, O., Thomas-Oates, J. E. & Brade, H. Preparation and structural analysis of oligosaccharide monophosphates obtained from the lipopolysaccharide of recombinant strains of Salmonella minnesota and Escherichia coli expressing the genus-specific epitope of Chlamydia lipopolysaccharide. *European journal of biochemistry / FEBS* **222**, 183-194, doi:10.1111/j.1432-1033.1994.tb18856.x (1994).

9 Garcia-Vello, P., Speciale, I., Di Lorenzo, F., Molinaro, A. & De Castro, C. Dissecting Lipopolysaccharide Composition and Structure by GC-MS and MALDI Spectrometry. *Methods in molecular biology* **2548**, 181-209, doi:10.1007/978-1-0716-2581-1_12 (2022).

10 De Castro, C., Parrilli, M., Holst, O. & Molinaro, A. Microbe-associated molecular patterns in innate immunity: Extraction and chemical analysis of gram-negative bacterial lipopolysaccharides. *Methods Enzymol* **480**, 89-115, doi:10.1016/S0076-6879(10)80005-9 (2010).

11 Leontein, K., Lindberg, B. & Lonngren, J. Assignment of absolute configuration of sugars by g.l.c. of their acetylated glycosides formed from chiral alcohols. *Carbohydr. Res.* **62**, 359-362 (1978).

12 Ciucanu, I. & Kerek, F. A simple and rapid method for the permethylation of carbohydrates. *Carbohydr. Res.* **131**, 209-217 (1984).
13 Speciale, I. *et al.* Liquid-state NMR spectroscopy for complex carbohydrate structural analysis: A hitchhiker's guide. *Carbohydr Polym* **277**, 118885, doi:10.1016/j.carbpol.2021.118885 (2022).
14 States, D. J., Haberkorn, R. A. & Ruben, D. J. A two-dimensional nuclear overhauser experiment with pure absorption phase in four quadrants. *J. Magn. Reson.* **8**, 286-292 (1982).
15 Stern, A. S., Li, K. B. & Hoch, J. C. Modern spectrum analysis in multidimensional NMR spectroscopy: comparison of linear-prediction extrapolation and maximum-entropy reconstruction. *Journal of the American Chemical Society* **124**, 1982-1993, doi:10.1021/ja011669o (2002).
16 Di Lorenzo, F. The lipopolysaccharide lipid A structure from the marine sponge-associated bacterium Pseudoalteromonas sp. 2A. *Antonie Van Leeuwenhoek* **110**, 1401-1412, doi:10.1007/s10482-017-0865-z (2017).
17 Ceroni, A. *et al.* GlycoWorkbench: a tool for the computer-assisted annotation of mass spectra of glycans. *Journal of proteome research* **7**, 1650-1659, doi:10.1021/pr7008252 (2008).
18 Damerell, D. *et al.* The GlycanBuilder and GlycoWorkbench glycoinformatics tools: updates and new developments. *Biol Chem* **393**, 1357-1362, doi:10.1515/hsz-2012-0135 (2012).
19 Domon, B. & Costello, C. E. A systematic nomenclature for carbohydrate fragmentations in FAB-MS/MS spectra of glycoconjugates. *Glycoconjugate journal* **5**, 397-409 (1988).
20 Ottman, N. *et al.* Genome-Scale Model and Omics Analysis of Metabolic Capacities of Akkermansia muciniphila Reveal a Preferential Mucin-Degrading Lifestyle. *Appl Environ Microbiol* **83**, doi:10.1128/AEM.01014-17 (2017).